A Spread-Spectrum Concept Combining Chirp Modulation and Pseudonoise Coding

MAX KOWATSCH, MEMBER, IEEE, AND JOHANN T. LAFFERL

Abstract—**This paper investigates the combination of chirp modulation and pseudonoise phase shift keying for spread-spectrum transmission of digital data. Data encoding is accomplished by assignment of positive and negative dispersive slope chirps for binary ones and zeros. Each chirp is then modulated by one period of a PN signature sequence. The performance in additive white Gaussian noise is analyzed, measures of performance being mean acquisition time, mean hold-in time, and bit error probability. Calculated and experimental results are presented for a 105 kbit/s modem. In the test system, SAW dispersive delay lines with a bandwidth of 16.4 MHz and 9.5 μs dispersion time serve for the key operations of chirp generation and pulse compression, and the signature codes are 127 bit m-sequences.**

I. Introduction

LINEAR frequency modulated (linear FM, chirp) signals and the associated technique of pulse compression have been extensively used in radar systems [1]. The inherent capability of interference rejection makes this modulation scheme also a candidate for use in spread-spectrum type communication systems [2], a significant advantage being low Doppler sensitivity. A number of authors have proposed chirp signals for the representation of binary data by assignment of positive and negative dispersive slopes for ones and zeros [3]–[5], and various applications such as high-frequency (HF) data transmission [6] and air–ground communication via satellites [7], [8] have been reported. Theoretical investigations of the relative utility of linear FM can be found in papers by Zaytsev and Zhuravlev [9], Berni and Gregg [10], and Hirt and Pasupathy [11].

Increasing interest in chirp signaling is motivated by the development of high-performance surface acoustic wave (SAW) devices, which provide a near-optimum way for both generation and correlation (compression) of wide-band chirp pulses [12]. SAW technology offers the potential for the implementation of spread-spectrum modems with low complexity for certain types of military systems where protection against jammers is the task [13]. Substantially improved antijam performance has been obtained by combining the chirp technique with some kind of pseudorandom coding, e.g., by variation of the chirp center frequency according to a code sequence [14].

In those cases of spread-spectrum communications where the capability of selective addressing a large number of potential users operating in a common band-limited channel is important, the degree to which any two waveforms out of a selected signal set are correlated must be considered. Cook [15] has examined the class of linear FM signals in this context and proposed several techniques for the expansion of the signaling capability.

We have investigated a different way to overcome the limited waveform variability of chirps in a restricted time–frequency region: the combination of chirp modulation with pseudonoise (PN) phase shift keying (PSK). In the open literature, this technique, hereafter termed PN-chirp, was first suggested independently by Baier *et al.* [16] as a matched filter approach and by the authors [17] with external PSK modulation. Obviously, a fixed tap matched filter offers a convenient way for processing a particular PN-chirp signal, a significant advantage of this waveform being its lower Doppler sensitivity compared to purely PN-PSK [16]. However, full exploitation of the waveform variability would require the use of programmable matched filters. These are rather complex devices, which are not commonly available. Thus, we have chosen the combination of standard linear FM SAW dispersive delay lines (DDL) and an external code modulator, offering high flexibility, which has yet to be traded with increased hardware complexity due to the required synchronization.

The present paper is organized as follows. Section II introduces the fundamental waveform definitions. The system concept is outlined in Section III, followed by an analysis of the performance in an additive white Gaussian noise (AWGN) channel in Sections IV and V, including a simplified code division multiple access (CDMA) configuration. Finally, in Section VI, computed results for a specific system design are presented together with some experimental data on the laboratory test performance of a prototype modem.

II. Waveform Definitions

The general expression for a PN-chirp (Fig. 1) with center frequency f_o and duration T is given by

$$s_c(t) = c(t) \cdot s(t) = \begin{cases} \sum_{i=0}^{N-1} c_i P_i(t) \cos\left[2\pi\left(f_o t + \mu \frac{t^2}{2}\right)\right], \\ \qquad -T/2 = -\frac{NT_c}{2} < t < T/2 = \frac{NT_c}{2} \\ 0, \qquad \text{elsewhere} \end{cases} \tag{1}$$

where $P_i(t)$ is a unity height pulse of fixed duration T_c

$$P_i(t) = \begin{cases} P\left[t - \left(-\frac{N}{2} + i\right)T_c\right] = 1, \\ \qquad (-N/2 + i)T_c < t < (-N/2 + i + 1)T_c \\ 0, \qquad \text{elsewhere.} \end{cases} \tag{2}$$

Paper approved by the Editor for Communication Theory of the IEEE Communications Society for publication without oral presentation. Manuscript received July 2, 1982; revised May 6, 1983. This work was supported by the Austrian Science Research Fund Project S-22/11.

The authors are with the Abteilung für Angewandte Elektronik, Institut für Allgemeine Elektrotechnik und Elektronik, Technische Universität Wien, A-1040 Vienna, Austria.

0090-6778/83/1000-1133$01.00 © 1983 IEEE

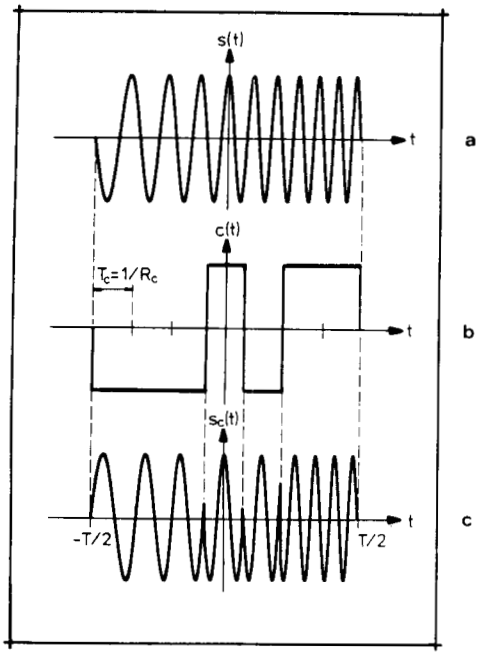

Fig. 1. Sketch of basic waveforms. (a) Up-chirp pulse. (b) 7-bit PN code. (c) PN-chirp signal.

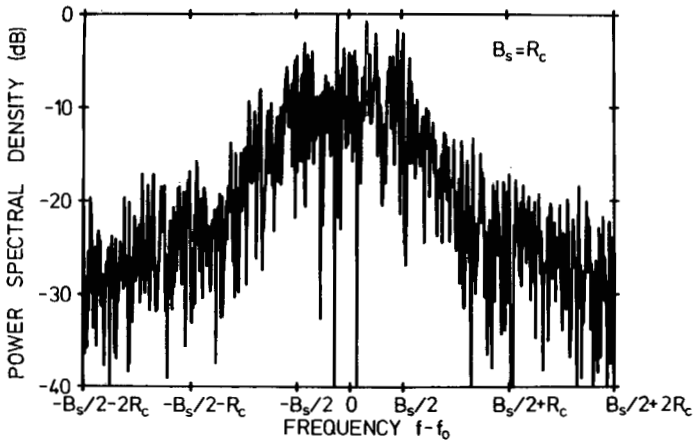

Fig. 2. Power spectrum of PN-chirp.

The binary sequence $\{c_i = \pm 1\}$ of amplitudes of the code waveform $c(t)$ is a PN sequence (maximal-length sequence, m-sequence) with period $N = 2^n - 1$, which is generated by a linear feedback shift register of length n [18], [19]. Each code element is commonly called a chip and $R_c = 1/T_c$ is the chip rate. Given a particular sequence length, different users of a transmission channel can be addressed by selecting different feedback connections and initial states of the register. This will be explained in Section III.

The factor μ is called dispersive slope. By choosing $\mu_1 = B_s/T$ (up-chirp) and $\mu_2 = -B_s/T$ (down-chirp) two PN-chirps with sweep bandwidth B_s are defined, which form a signal set for the representation of binary data.

We shall now consider the power spectral density of the transmitted waveform $s_c(t)$. The shape of the power spectrum depends on the ratio of chirp bandwidth B_s to chip rate R_c [17]. By inspection of Fig. 2, which is a computer simulation for $B_s = R_c$, no general measure of bandwidth is obvious. It is of interest to examine the relative signal power in any specified band B centered at f_o, in order to evaluate the signal power loss due to band limiting in the receiver RF section. Fig. 3 gives plots of the percent power containment for three different ratios B_s/R_c. Here, bandwidth is measured

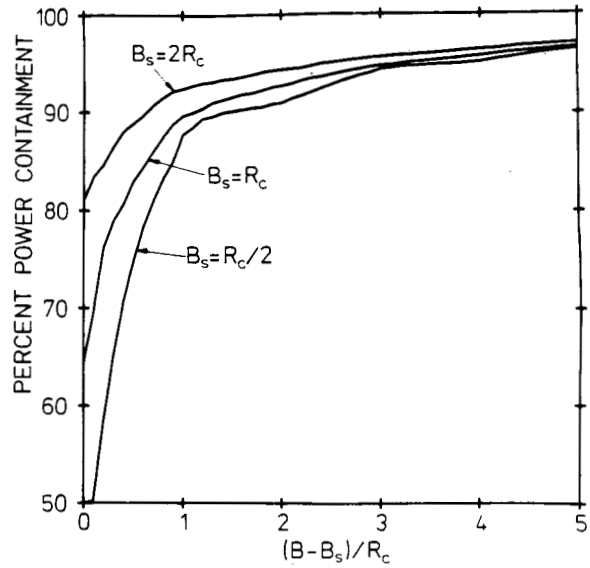

Fig. 3. Relative signal power versus normalized bandwidth.

in multiples of R_c by which B exceeds B_s, the chirp bandwidth B_s being the bandwidth of the receiver pulse compression filters at the output of the reference code modulator.

In the receiver, the waveform $s_c'(t)$ is multiplied by a local replica of the code $c_r(t)$. Subsequently, the remaining chirp $s'(t)$ is applied to two parallel pulse compression filters (matched filters, MF) for noncoherent data detection. The primed variables indicate bandpass filtering in the receiver RF section. Assuming the local code to be perfectly synchronized with the received waveform, and neglecting the effect of bandpass filtering at the moment, the output signal $g(t)$ of the corresponding MF for a single chirp input is given by [1]

$$g(t) = \begin{cases} \sqrt{TB_s}\,\dfrac{\sin\left[\pi B_s t\left(1-\dfrac{|t|}{T}\right)\right]}{\pi B_s t}\cos(2\pi f_o t), & -T < t < T \\ 0, & \text{elsewhere} \end{cases} \tag{3}$$

which describes a $\sin x/x$-like pulse of duration $2T$. Most of the chirp energy is contained in the main lobe of -4 dB width $1/B_s$. As a consequence, the peak amplitude is increased over the chirp amplitude by the factor $\sqrt{TB_s}$, and this results in an improvement of the peak signal-to-noise ratio relative to the MF input (where we assume noise band limited to B_s), which we will call compression gain G_c defined by

$$G_c = 10 \log (TB_s) \text{ (dB)}. \tag{4}$$

The effect of RF band limiting is a signal power loss, which for a sharp cutoff bandpass filter of unity gain can be estimated from Fig. 3. Assuming filter phase distortions to be negligible, the correlation loss is equal to the signal power loss.

III. Basic System Concept

The block diagram of the transmitting section of the PN-chirp modem is shown in Fig. 4. Depending on logic one or zero at the data input, an up-chirp or a down-chirp is generated by impulsing a SAW dispersive delay line (DDL). After amplification, the two channels are combined to a continuous

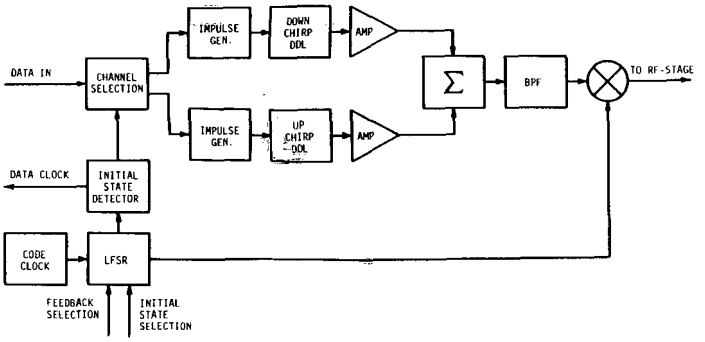

Fig. 4. Transmitter of PN-chirp system.

IF signal, which is modulated by a repetitive PN code with a period equal to the chirp duration. This signature sequence is generated by means of a linear feedback shift register (LFSR) with programmable feedback and initial state. The code clock is free running. The data clock is generated by detecting the periodic occurrence of the specified initial state, which also triggers the impulse generators. In this way, a fixed relationship between chirp and code is established, and selection of different initial states causes cyclic shifts of the periodic m-sequence relative to the chirp. This allows a large number of programmable waveforms to be synthesized for each feedback, using different cyclic shifts or phases of the PN-code just by changing the initial state of the LFSR. Thus, selective addressing of many cochannel communicators is possible, even with relatively short codes.

In the receiver (Fig. 5) the code-related phase transitions have to be removed by modulation with a synchronous code replica prior to matched filtering of the chirp pulses. The time gating following envelope detection minimizes the effect of interference. Moreover, it allows discrimination between received waveforms with different phases of the same PN-code as signature sequences. For any specified initial state, the compressed pulse must appear at the MF output with a known delay relative to the occurrence of this register state. This information is used to ensure that the receiver will lock only on a signal bearing the correct signature sequence. The width of the time window is approximately equal to the main lobe of the compressed pulse, that is, $2/B_S$. The number of unambiguously detectable waveforms for a particular feedback depends on the ratio B_S/R_C.

For code coarse synchronization, serial search of the relative code positions in discrete steps of $T_c/4$ is employed. This is implemented by digitally controlling the receiver clock in a way that in each code period, exactly one chip is shorter by $T_c/4$, until the synch detector declares acquisition of synchronization. The synch decision is based on the up-down-counter search/lock strategy (SLS) proposed by Hopkins [20]. This SLS is shown in Fig. 6. It is important to note that the integration time in each search cell in our particular case is fixed by the chirp duration T. If the count reaches 3, tracking is activated.

For code tracking, a tau-dither loop is employed [2], [22]. The loop operates with a time-continuous input waveform, which is obtained by means of a sample-and-hold circuit. In the experiment, this proved to be advantageous because of the low duty factor $2/(B_S T)$ of the gated pulsed signal at the envelope detector output. Without the sample-and-hold circuit, the loop error signal is only a very weak spectral component of this waveform, being more difficult to process. Code dithering is implemented by incremental phase modulation (IPM). The code clock is derived from a voltage controlled oscillator, with a fixed control voltage applied in the search mode.

The final data decision is based on the comparison of the signal levels in the two channels, sampled at the center of the time window.

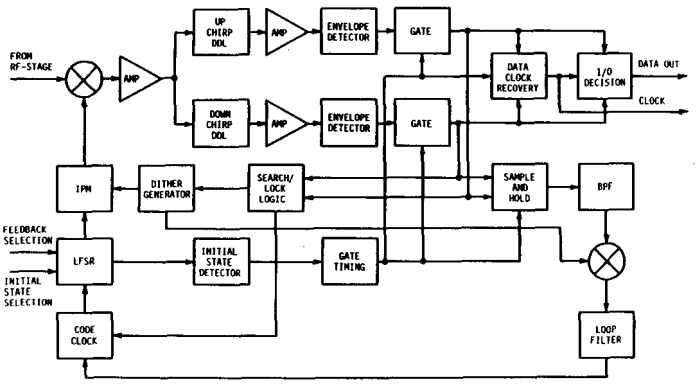

Fig. 5. Receiver of PN-chirp system.

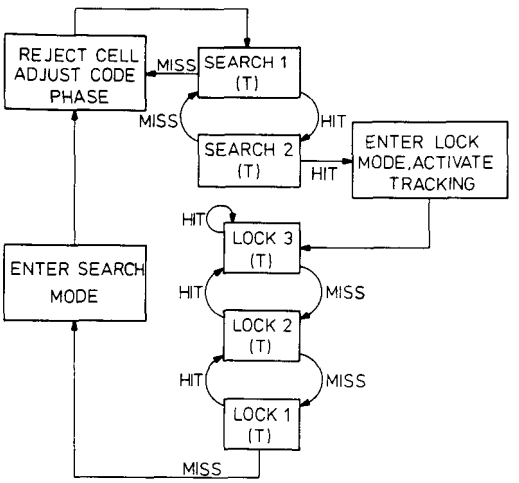

Fig. 6. Search/lock strategy.

IV. Performance in AWGN Channel

In this section, we will investigate the performance of the transmission system, if the received signal is corrupted by additive white Gaussian noise. It will be assumed that band limiting to B_{RF} happens at the receiver front end. The relevant measures of performance are mean acquisition time, mean hold-in time, and bit error probability, the basis for all considerations being the signal- (S) to-noise (N) power ratio γ_{in} at the input of the receiver reference code modulator

$$\gamma_{in} = (S/N)_{in}. \tag{5}$$

For all calculations to follow, we need the peak signal-to-noise

ratio γ_{out} at the compression filter output, which is modeled by

$$\gamma_{out} = (S_p/N)_{out} = \frac{\gamma_{in} B_{RF} \beta T B_s}{B_s S_n} \tag{6}$$

or in dB

$$\gamma_{out} = \gamma_{in} + G_p \tag{7}$$

with the processing gain G_p

$$G_p = 10 \log \left(\frac{B_{RF}\beta}{B_s S_n} \right) + G_c. \tag{8}$$

The factor S_n allows for the scaling of the noise spectral density due to the noise spreading caused by the receiver reference code multiplication ($S_n < 1$). Of course, the noise spectral density is no longer constant, but for simplicity we will calculate its value at center frequency f_o and assume it to be constant at least over the MF bandwidth B_s. The modulator output noise spectrum is given by the convolution of the input noise spectrum and the code spectrum. For the assumption of an ideally rectangular RF bandpass filter, the scaling factor S_n is simply obtained by computing the relative code power containment within the bandwidth B_{RF} centered at f_o. The correlation loss which is caused by unavoidable deviations from perfect synchronization is considered by the factor $\beta (\beta < 1)$. The value of β depends on the actual parameters of the code tracking loop.

The analysis of the acquisition and hold-in performance requires first to determine the probabilities of detection P_d and false alarm P_{fa}.

A. Probability of Detection and Probability of False Alarm

The probability of noncoherent detection of a compressed pulse is for a single channel [21]

$$P_{d,sc} = Q(\sqrt{2\gamma_{out}}, b_n \sqrt{2\gamma_{out}}) \tag{9}$$

where $Q(x, y)$ is the Marcum Q-function, and b_n is the detector threshold b normalized to the peak MF output

$$b_n = \frac{b}{\sqrt{2 S_{in} \beta T B_s}}. \tag{10}$$

The single channel false alarm probability $P_{fa,sc}$, which is the probability that detection of a compressed pulse is declared in the serial search process although the codes are out of synchronization, we approximate by [21]

$$P_{fa,sc} = Q\left(0, b_n \sqrt{\frac{2 S_{in} \beta T B_s}{N_t}}\right) = \exp\left(-\frac{b_n^2 S_{in} \beta T B_s}{N_t}\right) \tag{11}$$

with N_t denoting MF output noise power plus that portion rS_{in} of the power of the unsynchronized signal which is passed through the MF:

$$N_t = N_{in} S_n B_s / B_{RF} + r S_{in}. \tag{12}$$

In order to find a reliable numerical value for r, we have to calculate the spectrum of the code modulator output signal for the unsynchronized case (relative code shift more than one chip). The relative power containment in the MF-bandwidth B_s mainly depends on the position of the reference code relative to the received signal within a chip interval T_c and varies only slightly with the number of chips that the codes are out of synchronization. As an approximation for r, we compute the ensemble average of the signal power passed through the MF over a number of relative shifts within T_c. For large TB_s, however, the effect of signal power can be neglected in the computation of $P_{fa,sc}$.

Assuming the noise samples at the outputs of the two pulse compression filters to be uncorrelated for the large values of TB_s that are of interest for spread-spectrum applications [9], the overall probabilities of detection P_d and false alarm P_{fa} for the combined channels are given by

$$P_d = P_{d,sc}(1 - P_{fa,sc}) + P_{fa,sc}, \tag{13}$$

$$P_{fa} = 1 - (1 - P_{fa,sc})^2. \tag{14}$$

B. Mean Acquisition Time and Mean Hold-In Time

The determination of mean acquisition time $\bar{T}_{acq}$ and mean hold-in time $\bar{T}_h$ strictly follows the technique developed by Hopkins [20] from the theory of absorbing Markov chains. A detailed description of this method can also be found in the textbook on coherent spread-spectrum systems by Holmes [22]. Confidence estimates for T_{acq} and T_h have been obtained by Leung and Donaldson [23]. The Markov chain model corresponding to the SLS of Fig. 6 is shown in Fig. 7. The process is described by its transition matrix P

$$P = \left[\begin{array}{c:c} I & \phi \\ \hdashline R & Q \end{array}\right] \tag{15}$$

where I is an identity matrix, ϕ is a matrix of all zeros, Q contains the transition probabilities of the transient states (1–5 in Fig. 7), and R contains the transition probabilities from transient to absorbing states (0, 6).

The mean time to be absorbed from transient state i is given by the vector

$$\vec{\tau} = [I - Q]^{-1} \vec{\xi} \tag{16}$$

where the elements of $\vec{\xi}$ are the times required to make each transition, in our particular case the constant integration time T. Solution of (16) for τ_1 yields the mean dwell time T_D, which is the average time elapsed while testing a cell. The probabilities p_0 and p_1 have to be chosen for the "not in synch" condition.

Besides T_D, for the determination of $\bar{T}_{acq}$ the probability P_L of entering the lock mode is important. This quantity is the element B_{16} of the matrix B, which contains the probabilities B_{ij} of being absorbed at state j from initial state i, and is defined by

$$B = [I - Q]^{-1} R. \tag{17}$$

Here, p_0 and p_1 in Q and R are for the "in synch" condition. Given T_D and P_L, which for our particular case can be found in the appendix [(A3) and (A5)], the mean acquisition time is

$$\bar{T}_{acq} = \frac{N_s T_D}{2} \left(\frac{2 - P_L}{P_L} \right) \tag{18}$$

where N_s is the number of possible cells to be tested.

The mean hold-in time $\bar{T}_h$ is obtained by solving (16) for τ_3, and is also found in the Appendix [(A6)].

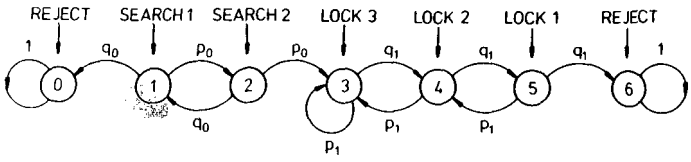

p_0=p (HIT/SEARCH MODE) = { SEARCH MODE P_{fa}, NOT IN SYNC. / SEARCH MODE P_d, IN SYNC. } $q_0 = 1 - p_0$

p_1=p (HIT/LOCK MODE) = { LOCK MODE P_{fa}, NOT IN SYNC. / LOCK MODE P_d, IN SYNC. } $q_1 = 1 - p_1$

Fig. 7. Markov chain model of search/lock strategy.

C. Probability of Error

Once synchronization has been achieved, data are demodulated with an error probability which is described by [24]

$$P_e = \tfrac{1}{2} \exp\left(-\frac{\gamma_{\text{out}}}{2}\right). \tag{19}$$

This is the well-known expression for the error probability of noncoherent orthogonal frequency shift keying (FSK). Of course, the chirp waveforms representing binary ones and zeros, respectively, are not strictly orthogonal. However, in [9] it is shown that the effect of nonorthogonality is negligible, provided $TB_s > 50$, as is the case in our application. Analytical expressions for the calculation of P_e, accounting for the effect of nonorthogonality in the lower TB_s region, have been given by Hirt and Pasupathy in [11].

V. CDMA Performance

The presented modulation technique is particularly advantageous for code division multiple access (CDMA) applications. Therefore, it is interesting to investigate the performance in a simplified CDMA configuration.

The analysis is based on the assumption that a particular user receives equal signal power S_{in} from M active cochannel users, one of which is the intended communicator. All users employ identical chirp waveforms for message representation, but different shift register feedback connections or initial states for generation of the signature sequences.

Analogous to the approximation in (12) for computation of P_{fa}, we consider the receiver MF output noise power in the equations of Section IV to be the sum of the band-limited white Gaussian noise power N_{in} of the channel and the total uncorrelated interference power $rS_{\text{in}}(M-1)$ which is passed through the MF:

$$N_t = N_{\text{in}} S_n B_s / B_{\text{RF}} + rS_{\text{in}}(M-1). \tag{20}$$

Thus,

$$\gamma_{\text{out}} = \frac{\gamma_{\text{in}} \beta T B_s}{S_n B_s / B_{\text{RF}} + r\gamma_{\text{in}}(M-1)}. \tag{21}$$

For computation of P_{fa}, the term $rS_{\text{in}}(M-1)$ in (20) is replaced by $rS_{\text{in}}M$.

VI. Results for Test System

The above analysis is now employed in predicting the performance of a PN-chirp modem which is characterized by the parameters in Table I. A breadboard version of this system was developed, and some experimental results will be shown for comparison. In these experiments, an AWGN communications channel was simulated by means of a noise generator and a variable attenuator.

TABLE I
PARAMETERS FOR TEST SYSTEM

Data rate:	105 kbit/s
Chirp bandwidth B_S:	16.4 MHz
Chirp duration T:	9.5 μs
Codes:	127-bit m-sequences
Code rate R_C:	13.4 MHz
Receiver bandwidth B_{RF}:	35 MHz
Number of search cells N_S:	508

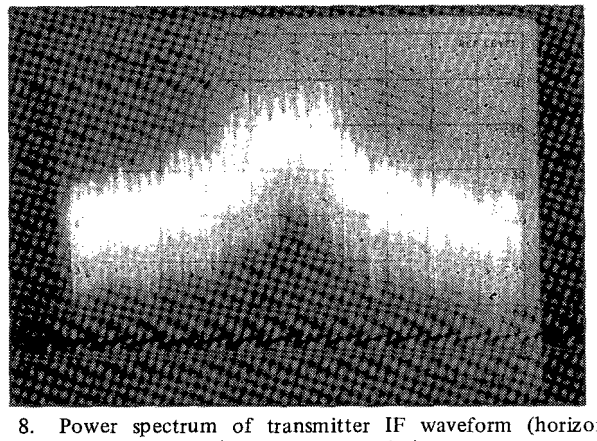

Fig. 8. Power spectrum of transmitter IF waveform (horizontal: 10 MHz/div.; vertical: 10 dB/div.).

For chirp generation and pulse compression, SAW dispersive delay lines with center frequency $f_o = 60$ MHz are used. Measured processing gain G_P is about 24 dB. The power spectral density of the transmitter IF waveform, as observed on a spectrum analyzer, is shown in Fig. 8. Receiver operation is illustrated by Fig. 9 and Fig. 10. The top trace in Fig. 9 shows a receiver input signal imbedded in band-limited Gaussian noise ($\gamma_{\text{in}} = 0$ dB). The signal in the center trace is the detected compressed pulse. The gate pulse for the sync detection window is displayed in the bottom trace. The system reaction on CW (60 MHz) interference is demonstrated in Fig. 10. The input signal-to-interference power ratio SIR is −7 dB. Traces *b* and *c* indicate the merit of the decision window. Interference outside the short time interval in which the gate is open is ignored by the sync decision circuitry.

The error signal for the receiver tracking loop is generated by dithering the code with $\Delta = 0.1\ T_c$, the dither frequency being 5 kHz. The loop bandwidth B_L is 200 Hz. The expected maximum initial code clock deviation between transmitter and receiver is 50 Hz. In the experiment, relative clock frequency errors up to 150 Hz could be tracked. Inspection of Fig. 11, which shows the output signal of the sample-and-hold circuit for high γ_{in} (no noise inserted), gives insight into the operation of tau-dither tracking. It is important to note that pull-in of the loop takes many times the chirp duration or MF integration time T. Therefore, at very low γ_{in}, the imple-

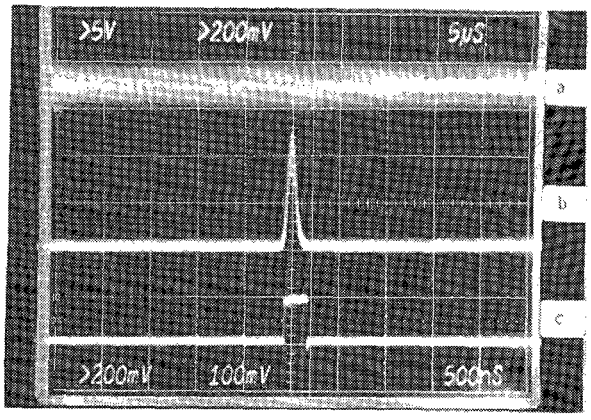

Fig. 9. System operation in the presence of band-limited white noise (horizontal: 500 ns/div.). (a) Receiver input waveform (γ_{in} = 0 dB). (b) Detected compressed pulse. (c) Time window pulse.

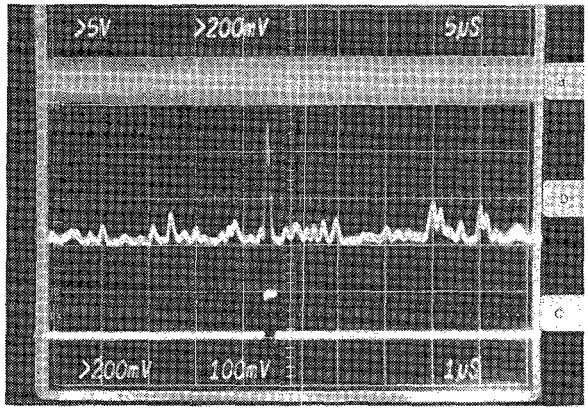

Fig. 10. System performance in the presence of CW interference (horizontal: 1 μs/div.). (a) Receiver input waveform (SIR = −7 dB). (b) Envelope detector output signal. (c) Time window pulse.

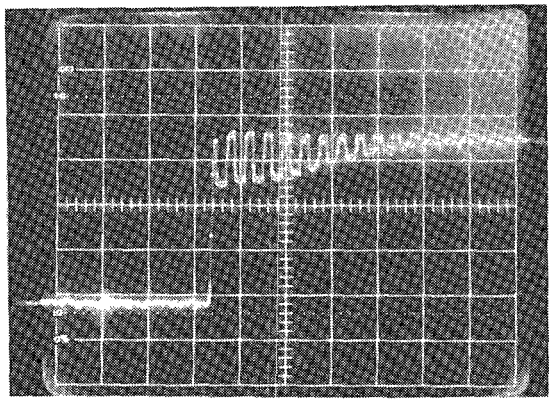

Fig. 11. Operation of tau-dither tracking loop (horizontal: 500 μs/div.).

mented SLS may cause the search/lock logic to declare loss of synchronization before the loop has locked.

According to the receiver bandwidth B_{RF} in Table I, the factor S_n in (6), (8), (12), and (21) is found by numerical calculation to be 0.91. To obtain a numerical value for β in the acquisition process, we consider the fact that for searching in steps of $T_c/4$ there will always exist one test

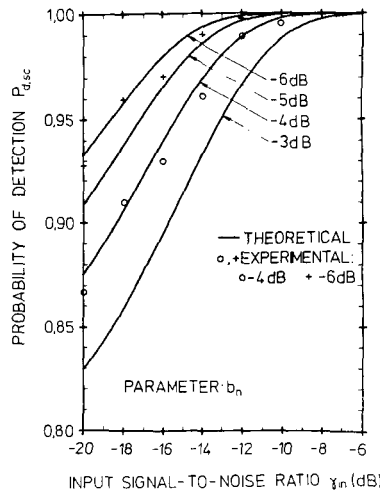

Fig. 12. Probability of detection $P_{d,sc}$ (S_n = 0.91, β = 0.8).

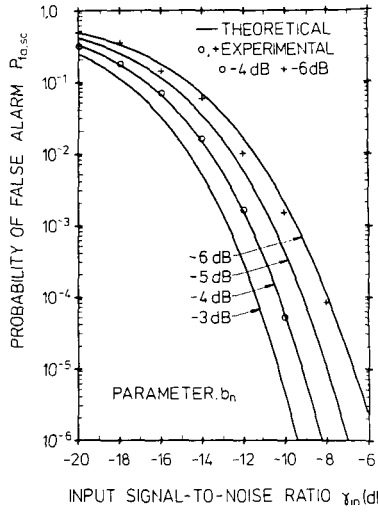

Fig. 13. Probability of false alarm $P_{fa,sc}$ (S_n = 0.91, β = 0.8, r = 0.65).

cell with a relative code shift of no more than $T_c/8$. Computation of β for the worst case yields 0.91, taking into consideration the effect of band limiting on the code correlation function. Here we make use of the simplifying assumption that only this one cell contains the correct correlation peak, although in fact a lower compressed pulse in an adjacent cell may be detected first. The lock mode value of β is 0.92, corresponding to the nominal tracking error $\Delta = 0.1\ T_c$. However, we have set β to 0.8 in all calculations to allow for an experimentally observed loss in compression gain G_c, resulting from amplitude and phase distortions in the SAW DDL responses which are due to device fabrication errors. Given the above values for S_n and β, the theoretical processing gain G_p is 24.6 dB. Further, we have to know the factor r in (12) and (21). Computer simulation yields $r = 0.65$.

The probability of detection $P_{d,sc}$ which is assumed equal in search and lock mode by letting β and the normalized threshold b_n be constant is shown in Fig. 12. The probability of false alarm $P_{fa,sc}$ is plotted in Fig. 13. In both figures, some measured data are indicated. The probability $P_{d,sc}$ is the conditional probability that a compressed pulse is detected when a signal was transmitted and the codes are synchronized. For its measurement, a fixed large number of equal PN-chirps

was applied to the input of the externally synchronized receiver and the detected compressed pulses in the corresponding channel were counted. The result was averaged over several measurements. Performance of the two channels is equal since they only differ in the sign of the DDL dispersive slope. The detection process in the two channels is independent, the combination being carried out by the sync decision logic. For the experimental determination of $P_{fa,sc}$, again a known number of PN-chirps was applied to the receiver input, but the reference code was forced to remain out of synchronization. The detections in this unsynchronized case were counted and compared to the number of possible detections, taking into consideration that one detection decision is possible in one code period. This is ensured by the gating arrangement in the receiver.

It is interesting to note the effect of the detector threshold level on mean acquisition time (Fig. 14) and mean hold-in time (Fig. 15). While $\bar{T}_h$ is strongly influenced by b_n, the effect on T_{acq} is not very significant over a wide range of γ_{in}. In order to illustrate the performance of the SLS, computed results for deciding on the basis of a single hit or miss are also shown (broken lines for $b_n = -6$ dB). The corresponding equations can be found in the Appendix [(A8)-(A10)]. The advantage of the SLS was verified in the experiment by observing the hold-in performance in the medium range of γ_{in}. At very low γ_{in}, however, synchronization will probably be lost again even before the tracking loop has locked, as mentioned before. In this situation, modifications of the SLS may be advantageous. In practice, this region is not of interest anyway, since the bit error probability is prohibitively high for most applications.

The bit error probability P_e in synchronized operation is shown in Fig. 16 where tracking jitter has been neglected in the calculation. The experimental results were obtained by transmitting random data, with the receiver externally synchronized, and comparing the demodulated message to the properly delayed original data stream. Measurements without an auxiliary external synchronization signal were also carried out. In the region of medium and high γ_{in}, the deviations from the curve in Fig. 16 were below 1 dB, which is within the expected measurement uncertainty. This indicates good performance of the tracking loop. At very low γ_{in} hold-in times are too short for reliable measurements.

Results on the performance in the simplified CDMA configuration of Section V are presented in Figs. 17–19 for a normalized threshold $b_n = -6$ dB. Finally, we have experimentally investigated the error probability P_e in dependence of γ_{in} for small numbers of users, which employ identical LFSR feedback connections but different initial states to generate their signature sequences. The results are shown in Fig. 20 together with the theoretical curves.

VII. Conclusion

We have investigated the combination of chirp modulation and PN coding for spread-spectrum transmission of binary data. Application of SAW devices offers a convenient means for generation and matched filter detection of wide-band FM signals, and by additional PN modulation, a large number of different waveforms can be synthesized with relatively short codes, which are rapidly synchronized.

A well-known advantage of linear FM pulse compression is the low sensitivity of the correlation peak to Doppler shifts. This still holds for PN-chirp signals, as long as code Doppler is negligible. The more severe effect with large Doppler frequency shifts is the associated time shift of the compressed pulse [1], which influences the gating in the receiver detection process. Moreover, with moving platforms, the received signal power will exhibit considerable variations with time, whereas we have assumed a gain-stable channel throughout the paper.

Appendix

Referring to Fig. 7, we obtain from (15) the matrix

$$P = \begin{array}{c} \\ 0 \\ 6 \\ 1 \\ 2 \\ 3 \\ 4 \\ 5 \end{array} \begin{array}{c} \begin{array}{cc} 0 & 6 \end{array} \\ \left[\begin{array}{cc:ccccc} 1 & 0 & 0 & 0 & 0 & 0 & 0 \\ 0 & 1 & 0 & 0 & 0 & 0 & 0 \\ \hdashline q_0 & 0 & 0 & p_0 & 0 & 0 & 0 \\ 0 & 0 & q_0 & 0 & p_0 & 0 & 0 \\ 0 & 0 & 0 & 0 & p_1 & q_1 & 0 \\ 0 & 0 & 0 & 0 & p_1 & 0 & q_1 \\ 0 & q_1 & 0 & 0 & 0 & p_1 & 0 \end{array}\right] \end{array} \begin{array}{c} \\ 0 \\ 6 \\ 1 \\ 2 \\ 3 \\ 4 \\ 5 \end{array} \tag{A1}$$

Thus, we have

$$[I-Q]^{-1} = \begin{bmatrix} \frac{1}{1-p_0q_0} & \frac{p_0}{1-p_0q_0} & \frac{p_0^2(1-p_1q_1)}{q_1^3(1-p_0q_0)} & \frac{p_0^2}{q_1^2(1-p_0q_0)} & \frac{p_0^2}{q_1(1-p_0q_0)} \\ \frac{q_0}{1-p_0q_0} & \frac{1}{1-p_0q_0} & \frac{p_0(1-p_1q_1)}{q_1^3(1-p_0q_0)} & \frac{p_0}{q_1^2(1-p_0q_0)} & \frac{p_0}{q_1(1-p_0q_0)} \\ 0 & 0 & \frac{1-p_1q_1}{q_1^3} & \frac{1}{q_1^2} & \frac{1}{q_1} \\ 0 & 0 & \frac{p_1}{q_1^3} & \frac{1}{q_1^2} & \frac{1}{q_1} \\ 0 & 0 & \frac{p_1^2}{q_1^3} & \frac{p_1}{q_1^2} & \frac{1}{q_1} \end{bmatrix} \tag{A2}$$

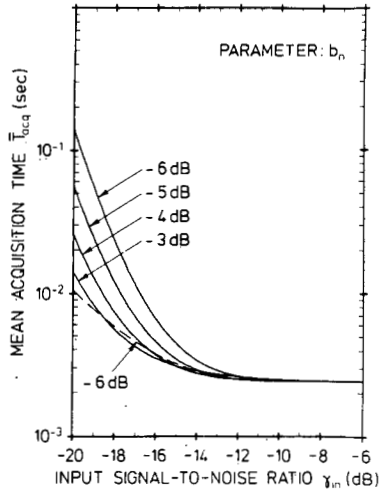

Fig. 14. Mean acquisition time $\bar{T}_{acq}$ (S_n = 0.91, β = 0.8, r = 0.65, broken line for b_n = −6 dB: search/lock decision based on single hit or miss).

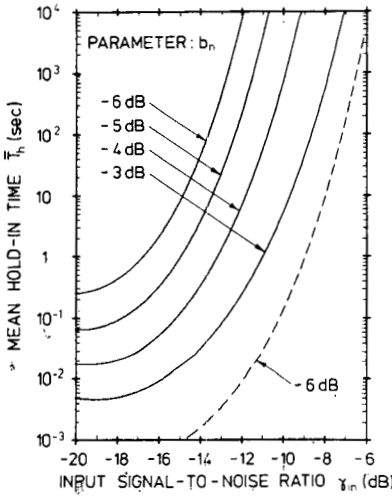

Fig. 15. Mean hold-in time $\bar{T}_h$ (S_n = 0.91, β = 0.8, r = 0.65, broken line for b_n = −6 dB: search/lock decision based on single hit or miss).

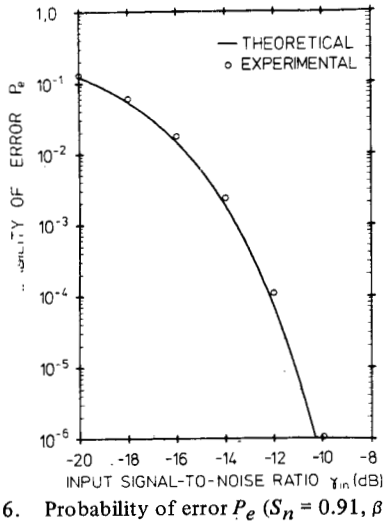

Fig. 16. Probability of error P_e (S_n = 0.91, β = 0.8).

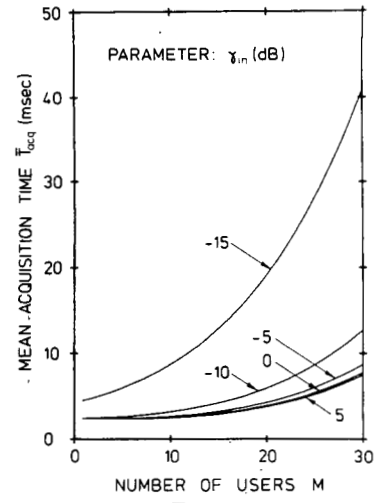

Fig. 17. Mean acquisition time $\bar{T}_{acq}$ in CDMA application (S_n = 0.91, β = 0.8, r = 0.65, b_n = −6 dB).

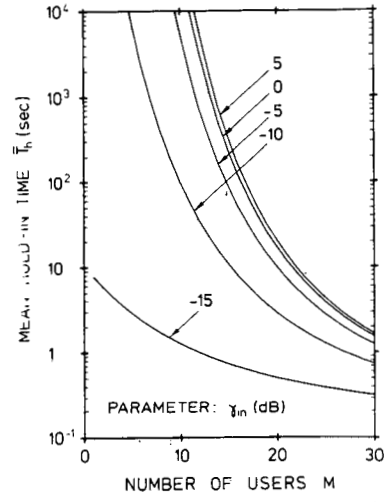

Fig. 18. Mean hold-in time $\bar{T}_h$ in CDMA application (S_n = 0.91, β = 0.8, r = 0.65, b_n = −6 dB).

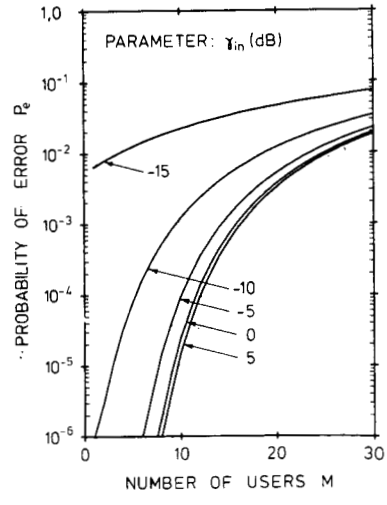

Fig. 19. Probability of error P_e in CDMA application (S_n = 0.91, β = 0.8).

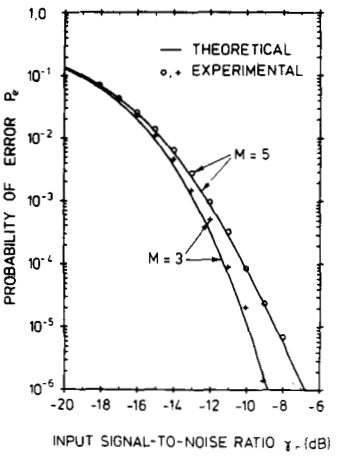

Fig. 20. Theoretical and experimental probability of error P_e for small number of users ($S_n = 0.91$, $\beta = 0.8$).

Letting $p_0 = p_1 = P_{fa}(Q_{fa} = 1 - P_{fa})$, and solving (16) for τ_1, we obtain the mean dwell time

$$T_D = \left(\frac{1 + P_{fa}}{1 - P_{fa}Q_{fa}} + \frac{(1 - P_{fa}Q_{fa} + Q_{fa} + {Q_{fa}}^2){P_{fa}}^2}{(1 - P_{fa}Q_{fa}){Q_{fa}}^3} \right) T. \tag{A3}$$

Further,

$$B = [I - Q]^{-1}R = \begin{array}{c} \\ 1 \\ 2 \\ 3 \\ 4 \\ 5 \end{array} \begin{array}{c} \begin{array}{cc} 0 & 6 \end{array} \\ \begin{bmatrix} \frac{q_0}{1 - p_0 q_0} & \frac{{p_0}^2}{1 - p_0 q_0} \\ \frac{{q_0}^2}{1 - p_0 q_0} & \frac{p_0}{1 - p_0 q_0} \\ 0 & 1 \\ 0 & 1 \\ 0 & 1 \end{bmatrix} \end{array} \tag{A4}$$

and the probability of entering the lock mode is the element B_{16} where $p_0 = P_d$ and $q_0 = 1 - P_d = Q_d$:

$$P_L = \frac{{P_d}^2}{1 - P_d Q_d}. \tag{A5}$$

The mean hold-in time $\bar{T}_h$ is the solution of (16) for τ_3, with $p_1 = P_d$ and $q_1 = Q_d$ in (A2):

$$\bar{T}_h = \frac{1 - P_d Q_d + Q_d + {Q_d}^2}{{Q_d}^3} T = \frac{1 + 2{Q_d}^2}{{Q_d}^3} T. \tag{A6}$$

Note that we have assumed P_d to be equal in the search and lock mode. Finally, we consider a synchronization process, in which the search/lock decision is based on a single hit or miss. This corresponds to omitting states 2, 4, and 5 in Fig. 7. Renumbering the remaining states, the transition matrix P of the process is

$$P = \begin{array}{c} \\ 0 \\ 3 \\ 1 \\ 2 \end{array} \begin{array}{c} \begin{array}{cccc} 0 & 3 & 1 & 2 \end{array} \\ \left[\begin{array}{cc:cc} 1 & 0 & 0 & 0 \\ 0 & 1 & 0 & 0 \\ \hdashline q_0 & 0 & 0 & p_0 \\ 0 & q_1 & 0 & p_1 \end{array}\right] \end{array} \tag{A7}$$

Proceeding in the same way as before, we obtain for this case

$$T_D = \tau_1 = \frac{T}{1 - P_{fa}}, \tag{A8}$$

$$P_L = B_{13} = P_d, \tag{A9}$$

and

$$\bar{T}_h = \tau_2 = \frac{T}{1 - P_d}. \tag{A10}$$

Acknowledgment

The authors are indebted to Prof. F. Seifert for many valuable discussions during the progress of this work and for critically reading the manuscript. They gratefully acknowledge G. Stangl for the careful fabrication of the SAW devices, A. Ersoy for circuit design and measurements, A. Baghai-Wadji for performing some of the calculations, and the Computer Center of the Vienna University of Technology for optimum access to computer facilities. Special thanks are due to the reviewers of this paper for their valuable suggestions.

References

[1] C. E. Cook and M. Bernfeld, *Radar Signals: An Introduction to Theory and Application*. New York: Academic, 1967.
[2] R. C. Dixon, *Spread Spectrum Systems*. New York: Wiley, 1976.
[3] M. R. Winkler, "Chirp signals for communications," in *IEEE WESCON Conv. Rec.*, 1962.
[4] E. K. Holland-Moritz, J. C. Dute, and D. R. Brundage, "Swept frequency modulation," *Proc. Nat. Electron. Conf.*, vol. 22, 1966, pp. 469–474.
[5] A. S. Griffiths and W. H. Smith, "FM 'chirp' communication: An easily instrumented multiple-access modulation format for dispersive channels," in *IEEE Int. Conf. Commun. Dig.*, 1967.
[6] G. F. Gott and J. P. Newsome, "H.F. data transmission using chirp signals," *Proc. Inst. Elec. Eng.*, vol. 118, pp. 1162–1166, Sept. 1971.
[7] G. W. Barnes, D. Hirst, and D. J. James, "Chirp modulation system in aeronautical satellites," in *AGARD Conf. Proc. No. 87 Avionics in Spacecraft*, Royal Aircraft Establishment, Rome, Italy, 1971.
[8] J. Burnsweig and J. Wooldridge, "Ranging and data transmission using digital encoded FM-chirp surface acoustic wave filters," *IEEE Trans. Sonics Ultrason.*, vol. SU-20, pp. 190–197, Apr. 1973.
[9] D. L. Zaytsev and V. I. Zhuravlev, "Noise immunity of a digital data transmission system using linearly frequency-modulated signals," *Telecommunications* (USSR), vol. 22, no. 4, pp. 13–17, 1968.
[10] A. J. Berni and W. D. Gregg, "On the utility of chirp modulation for digital signaling," *IEEE Trans. Commun.*, vol. COM-21, pp. 748–751, June 1973.
[11] W. Hirt and S. Pasupathy, "Continuous phase chirp (CPC) signals for binary data communication—Part I: Coherent detection and Part II: Noncoherent detection," *IEEE Trans. Commun.*, vol. COM-29, pp. 836–858, June 1981.
[12] *Surface Wave Filters: Design, Construction and Use*, H. Matthews, Ed. New York: Wiley, 1977.

[13] J. Otto, "Chirping RPV data links for ECM protection," *Microwaves*, pp. 54–60, Dec. 1974.
[14] H. Bush, A. R. Martin, R. F. Cobb, and E. Young, "Application of chirp SWD for spread spectrum communications," in *Proc. 1973 Ultrasonics Symp.*, pp. 494–498.
[15] C. E. Cook, "Linear FM signal formats for beacon and communication systems," *IEEE Trans. Aerosp. Electron. Syst.*, vol. AES-10, pp. 471–478, July 1974.
[16] P. W. Baier, R. Simons, and H. Waibel, "Chirp-PN-PSK-Signale als Spread-Spectrum-Signalformen geringer Dopplerempfindlichkeit und groβer Signalformvielfalt," *NTZ Archiv*, vol. 3, pp. 29–33, Feb. 1981.
[17] M. Kowatsch, F. J. Seifert, and J. Lafferl, "Comments on transmission system using pseudonoise modulation of linear chirps," *IEEE Trans. Aerosp. Electron. Syst.*, vol. AES-17, pp. 300–303, Mar. 1981.
[18] S. W. Golomb, *Shift Register Sequences*. San Francisco, CA: Holden-Day, 1967.
[19] M. B. Pursley and H. F. A. Roefs, "Numerical evaluation of correlation parameters for optimal phases of binary shift-register sequences," *IEEE Trans. Commun.*, vol. COM-27, pp. 1597–1604, Oct. 1979.
[20] P. M. Hopkins, "A unified analysis of pseudonoise synchronization by envelope correlation," *IEEE Trans. Commun.*, vol. COM-25, pp. 770–778, Aug. 1977.
[21] A. D. Whalen, *Detection of Signals in Noise*. New York: Academic, 1971.
[22] J. K. Holmes, *Coherent Spread Spectrum Systems*. New York: Wiley, 1982.
[23] V. C. M. Leung and R. W. Donaldson, "Confidence estimates for acquisition times and hold-in times for PN-SSMA synchronizer employing envelope correlation," *IEEE Trans. Commun.*, vol. COM-30, pp. 230–240, Jan. 1982.
[24] M. Schwartz, W. R. Bennett, and S. Stein, *Communication Systems and Techniques*. New York: McGraw-Hill, 1966.

★

Max Kowatsch (M'80) was born in Bad St. Leonhard, Austria, on January 11, 1953. He received the Dipl.Ing. and Dr.techn. degrees, both in electrical engineering, from the Vienna University of Technology, Vienna, Austria, in 1978 and 1981, respectively.

In 1978 he joined the Institut für Allgemeine Elektrotechnik und Elektronik at the Vienna University of Technology where he has been working in the areas of radar and spread-spectrum communications with special emphasis on application of surface acoustic wave devices.

Dr. Kowatsch is a member of the Austrian Physical Society (ÖPG).

★

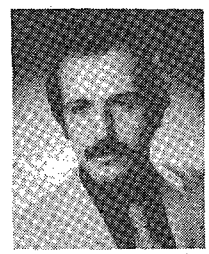

Johann T. Lafferl was born in Vienna, Austria, on October 13, 1954. He received the Dipl.Ing. and Dr.techn. degrees, both in electrical engineering, from the Vienna University of Technology, Vienna, Austria, in 1979 and 1982, respectively.

In 1978 he joined the Institut für Allgemeine Elektrotechnik und Elektronik at the Vienna University of Technology where he has been engaged in spread-spectrum applications for radio relay links. His current interests are in packet radio techniques and speech coding.